*Chapter 2*

# PHOTOLUMINESCENSE OF DEFECTS AND IMPURITIES IN SIC

## 2.1 Divacancies in 4H-SiC

Divacancies have 4 different configurations in the crystal lattice as shown in figure 2.1. They are associated with 4 different zero-phonon line (ZPL) labeled as PL1-4 shown in 2.2. ZPL emissions correspond to pure electronic transitions and often are observed with phonon-side-band (PSB) emission at higher wavelength that are phonon mediated transitions. As described in section 1.3, 4H-SiC has an elongated c-axis bonds. This makes a tetrahedron with one elongated bond parallel to c-axis with three identical bonds. If two adjacent defects occupy lattice sites parallel to c-axis, 120° rotations around c-axis still gives identical crystal configuration. c-axis divacancies have $C_{3v}$ symmetry. If two adjacent defects occupy sites that are not parallel to c-axis, out of 3 neighboring bonds of each defect, one neighboring bond corresponds to an elongated bond and a rotational symmetry is removed. Only reflection against the plane that is parallel to c-axis and to the two defect bond makes the crystal unchanged. Basal divacancies have $C_{1h}(C_s)$ symmetry.

A single neutrally charged divacancy has 6 active electrons, 3 from nearby carbons and 3 from nearby silicons. From molecular orbital theory and ab initio density functional calculations, electrons in $C_{3v}$ symmetry occupy orbital states $a_1^2 a_1^2 e^2$, which generates orbital singlet spin triplet $^3A_2$, orbital doublet spin singlet $^1E$, and orbital/spin singlet $^1A_1$ in the order of the lowest energy level first [41–43]. The next excited state is $a_1^2 a_1^1 e^3$, which generates $^3E$ and $^1E$ levels. ZPL of c-axis divacancies (PL1,2) is associated with spin allowed transitions $^3E \longrightarrow {}^3A_2$ [44]. In reduced $C_{1h}$ symmetry, E level splits into A' and A" levels. ZPL of basal divacancies (PL3,4) is associated with $^3A' \longrightarrow {}^3A$" [45]. Due to the fully allowed transition, the optical lifetime of the excited state of PL1-4 divacancies is relatively short, ~15 ns[46]. The energy diagram for c-axis and basal divacancies is shown in figure 2.3. Two spin singlet states lying between spin triplet excited and ground state of ZPL transition are coupled to spin triplet states with spin orbit coupling. Intersystem crossing between excited spin triplet state to singlet and then to ground spin triplet state is considered as main cause of spin dependent luminescence observed in magnetic

resonance (3.1)[47]. The Debye-Waller factor, the fraction of emission in ZPL out of the total emission is only ~5% [33].

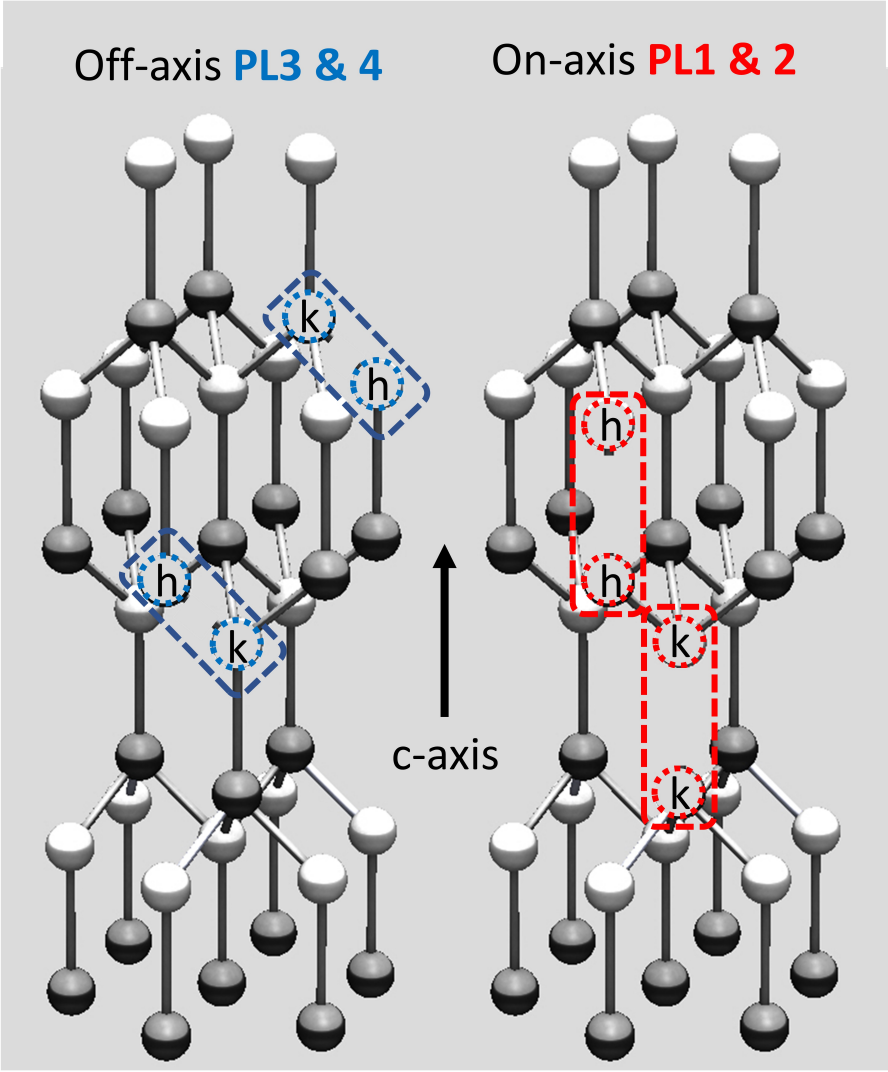


Figure 2.1: 4 types of divacancies that occupy different carbon/silicon lattice sites.

## 2.2 $Cr^{4+}$ ions in 4H, 6H-SiC

$Cr^{4+}$ ions show different ZPL depending on the substitutional locations of Cr ions in SiC. As mentioned in 1.3, 4H-SiC has 2 inequivalent lattice sites (h) and (k) that experience different crystal field. 6H-SiC have 3 of those. For 4H-SiC, $Cr_A$ corresponds to Cr ions occupying quasi-cubic (k) sites with $T_d$ symmetry that emit ZPL observable at ~1070 nm. $Cr_C$ corresponds to those at hexagonal sites (h) with ZPL observable at ~1042 nm [48]. Symmetry of $Cr_C$ is reduced to $C_{3v}$ due to

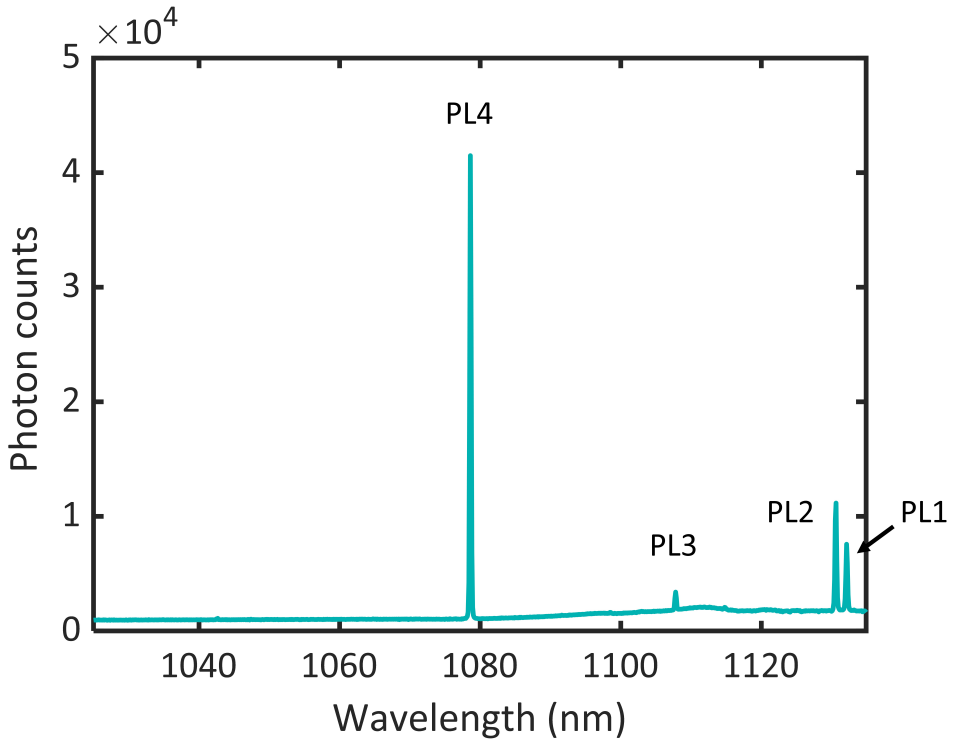


Figure 2.2: Photoluminescence of divacancies in a HPSI 4H-SiC sample excited by 780nm laser at 8.4 K.

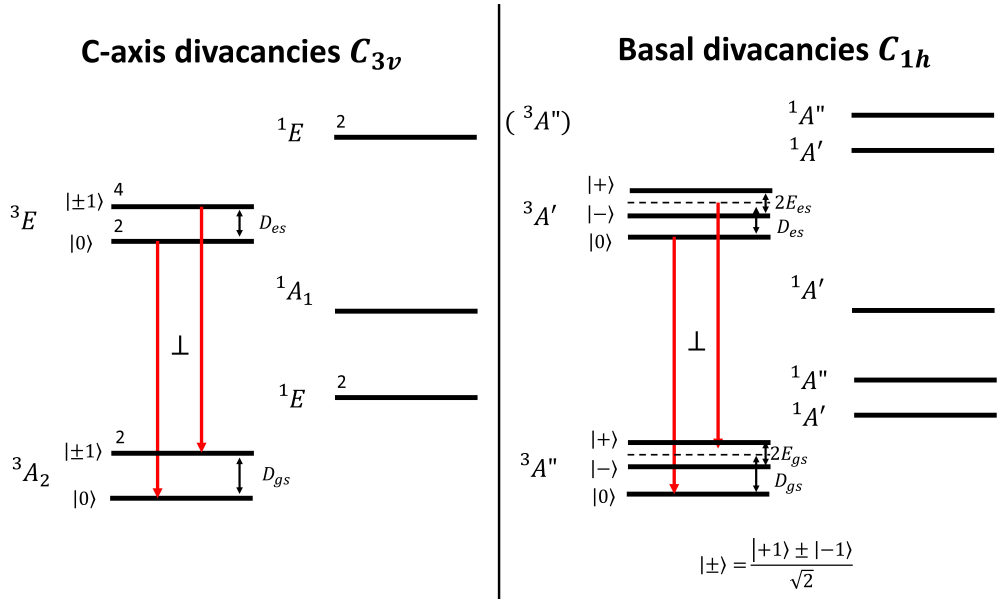


Figure 2.3: c-axis and basal divacancy energy level structure in 4H-SiC for $C_{3v}$ and $C_{1h}$ symmetry. Marks next to the red arrows specify the polarization of electric field with respect to c-axis for electric dipole allowed transitions.

elongated bond in the direction of c-axis as mentioned in 1.3. ZPL of Cr ions with intrinsic divacancies in Cr implanted HPSI 4H-SiC is shown in figure 2.4. Higher resolution ZPL of $Cr^{4+}$ in 4H and 6H-SiC is shown in figure 2.5. $Cr^{4+}$ in 6H-SiC were doped during the crystal growth process and ZPL peaks are much sharper than those in 4H-SiC due to less sample damage.

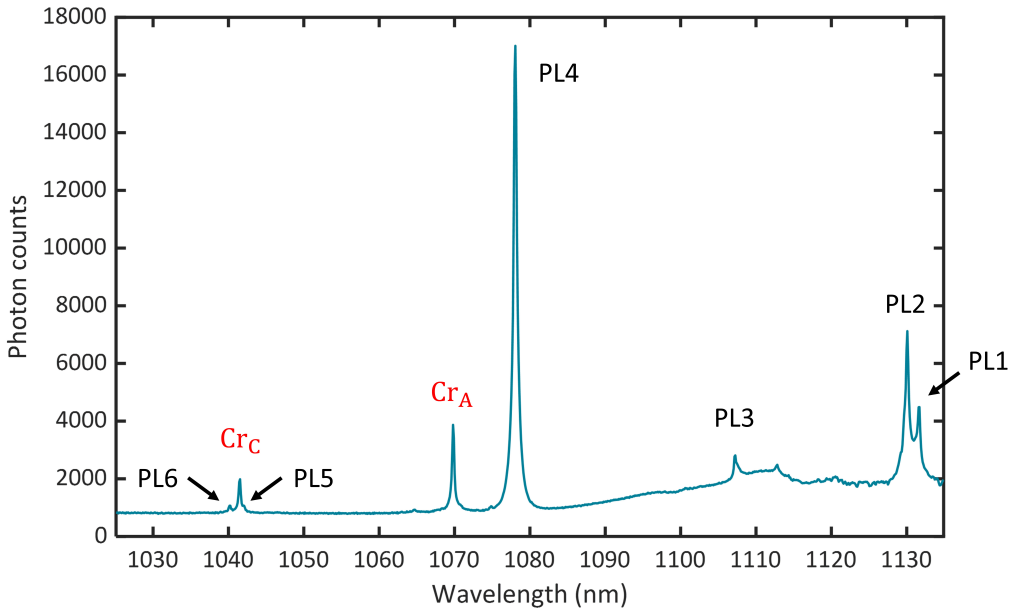


Figure 2.4: Photoluminescence of Cr ions and divacancies in a Cr implanted 4H-SiC sample excited by 780nm laser at 8.6 K.

The electron configuration for $Cr^{4+}$ is 2 electrons in 3d shell ($3d^2$). Using group theory [49–51], we can determine the ground state and other existing states of free ions. For free ions having $3d^2$ configuration, the ground state is ${}^3F$, where left upperscript denotes spin multiplicity 2S+1 (S: total spin angular momentum). The next excited state depends on how much crystal field the ions feel in the crystal and the energy of taking each state changes according to the field strength. Group theory can determine how states of free spherical ions split when the symmetry is lowered with crystal field. In tetrahedral $T_d$ symmetry, ${}^3F \longrightarrow {}^3A_2 + {}^3T_1 + {}^3T_2$ as generating methods described in section 9.3 of Cotton [51]. A(B), E and T are Mulliken symbol that means 1, 2 and 3-dimensional irreducible representations of certain symmetry group, where the dimension corresponds to orbital degeneracy of states. For example, ${}^3T_2$ means orbital triplet and spin triplet, 9 states in total.

To know which of these is ground state and the next excited state, Racah parameters B,C and crystal field splitting parameter Dq needs to be measured based on

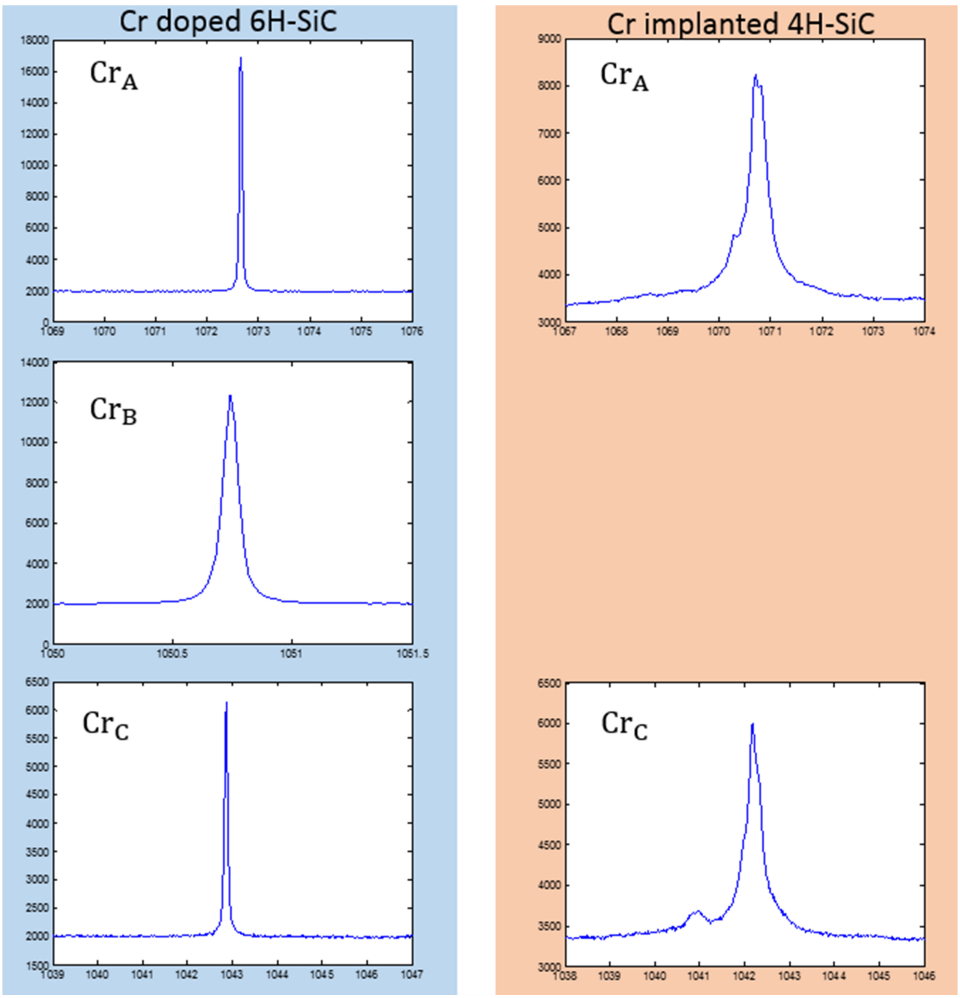


Figure 2.5: Photoluminescence of Cr ions in 4H-SiC and 6H-SiC samples in better resolution at liquid nitrogen temperature ( 80 K)

spectroscopy experiments. Derived parameters combined with Tanabe-Sugano formalism are often used to show the summary of energy of states vs. crystal field for complex metal ions [52]. From Tanabe-Sugano diagram for $Cr^{4+}$ we can determine its ground state to be $^3A_2$(F) and the next excited state to be either $^3T_2$(F) or $^1E$(D)[53, 54]. Zeeman splitting measurements were performed to conclude the next excited state is actually $^1E$ because each ZPL of spin triplet component of $^3A_2$ only splits to doublet excluding the possibility of $^3T_2$ with S=1 [48]. $Cr^{4+}$ is in relatively high field system for 4H and 6H-SiC. ZPL of $Cr^{4+}$ is associated with transition $^1E \longrightarrow ^3A_2$.

The energy diagram of $Cr^{4+}$ ions is shown in figure 2.6. $Cr_A$ with $T_d$ symmetry and $Cr_C$ with $C_{3v}$ symmetry theoretically has the same energy level degeneracy when only the crystal field is considered. With spin orbit coupling in $C_{3v}$ symmetry,

ground state $m_s = \pm 1$ states ($\Gamma_3$) and $m_s = 0$ become non degenerate. The electric dipole selection rule is shown next to red arrows. ZPL comes from spin forbidden but orbitally allowed transition.

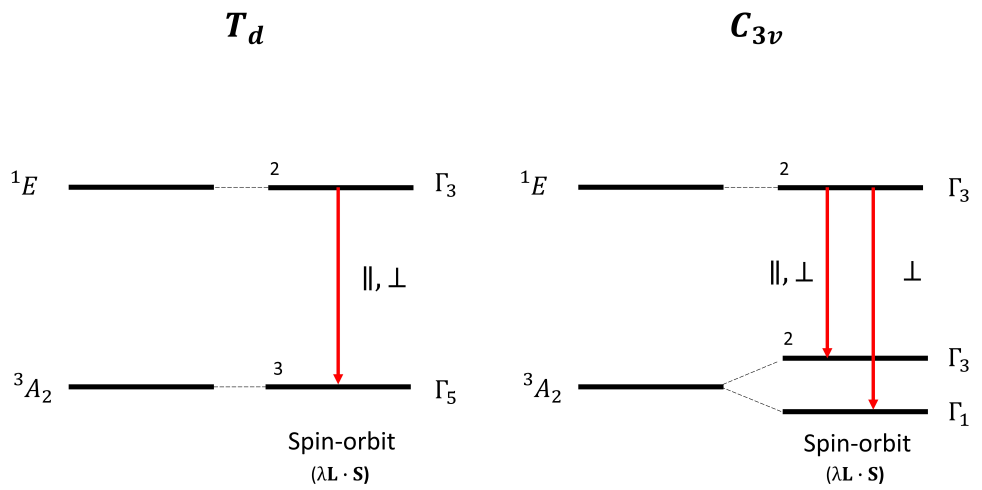


Figure 2.6: $Cr^{4+}$ energy level structure in 4H and 6H-SiC for $T_d$ and $C_{3v}$ symmetry. ZPL of $Cr^{4+}$ is associated with the transition $^1E \longrightarrow {}^3A_2$. The number at left on level bars denotes state degeneracy and $\Gamma$ specifies the irreducible representation of corresponding symmetry group. Marks next to the red arrows specify the polarization of electric field with respect to c-axis for electric dipole allowed transitions.

The lifetime of $Cr^{4+}$ ZPL is in the order of 10 - 100 $\mu$s depending on the doping condition. The relatively long optical lifetime is expected for spin forbidden transitions that require spin flips. The photoluminescense decay profile from the excited state to the ground state can be measured by accumulating the timing of each emitted photon after excitation, expressed by $I(t) = I_o exp(-t/\tau)$. $\tau$ is the optical lifetime and $I_o$ is the photon counts right after the excitation in the first time bin. The PL decay curve of the lifetime measurement is shown in figure 2.7. The goodness of the fit was assessed by the zero offset and symmetry of the residual of the fit in figure 2.8. The table 2.9 shows the measured lifetime on implanted 4H-SiC samples (originally vanadium doped SI or highly purified SI wafer) and on doped 6H-SiC samples. There is not much difference in lifetime between Cr ions at different sites. At LHe temperature, Cr ions in 6H-SiC have lifetime $150\mu s$ that is close to the values observed in doped 4H-SiC [55]. This 6H-SiC is expected to have the least damage and longest lifetime in the crystal compared to other 4H-SiC samples.

The inhomogeneous spin coherence time $T_2^*$ of $Cr^{4+}$ in 4H-SiC was recently mea-

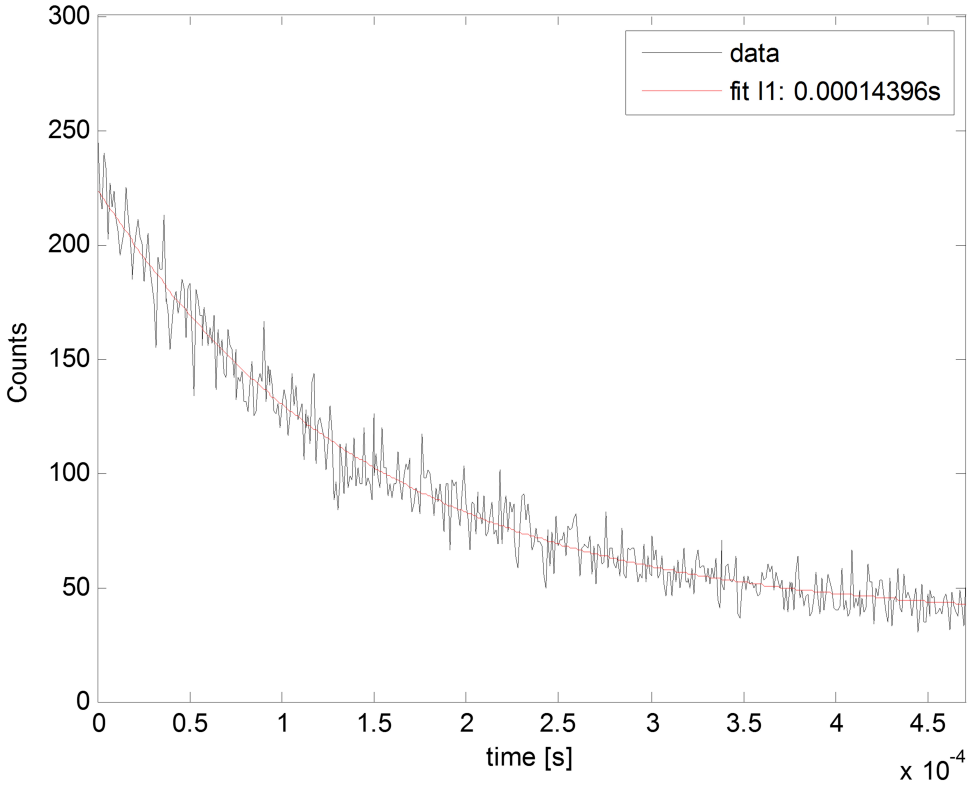


Figure 2.7: Optical lifetime measurement of $Cr^{4+}$ ions in doped 6H-SiC at liquid helium temperature. The fitting function is $I_o exp(-t/\tau)$ and reveals optical lifetime of 144 $\mu$s.

sured to be 37 ns. [55].This result was published at the same period when I was looking into optical properties of $Cr^{4+}$ ZPL. Due to this short coherence time, divacancies are more promising candidates as qubits so we will focus on them in later chapters.

## 2.3 Other color centers

Besides the previous divacancies and Cr ions I discussed, I also measured optical spectra and looked at some other color centers such as Vanadium, Molybdenum ions in SiC and Cu in Si. In this section, they are briefly reviewed.

### $V^{4+}$ ions in 4H-SiC

Conventionally, vanadium is doped in SiC as minority carrier lifetime killer to create semi insulating SiC wafer [56]. Depending on the position of the Fermi level, vanadium ions exist in either $V^{3+}$, $V^{4+}$, $V^{5+}$ form[57][58]. In our semi insulating 4H-SiC samples, $V^{4+}$ ions ZPL was observed as shown in figure 2.10. ZPL associated with (h) sites is labeled as $\alpha$ lines and can be observed around

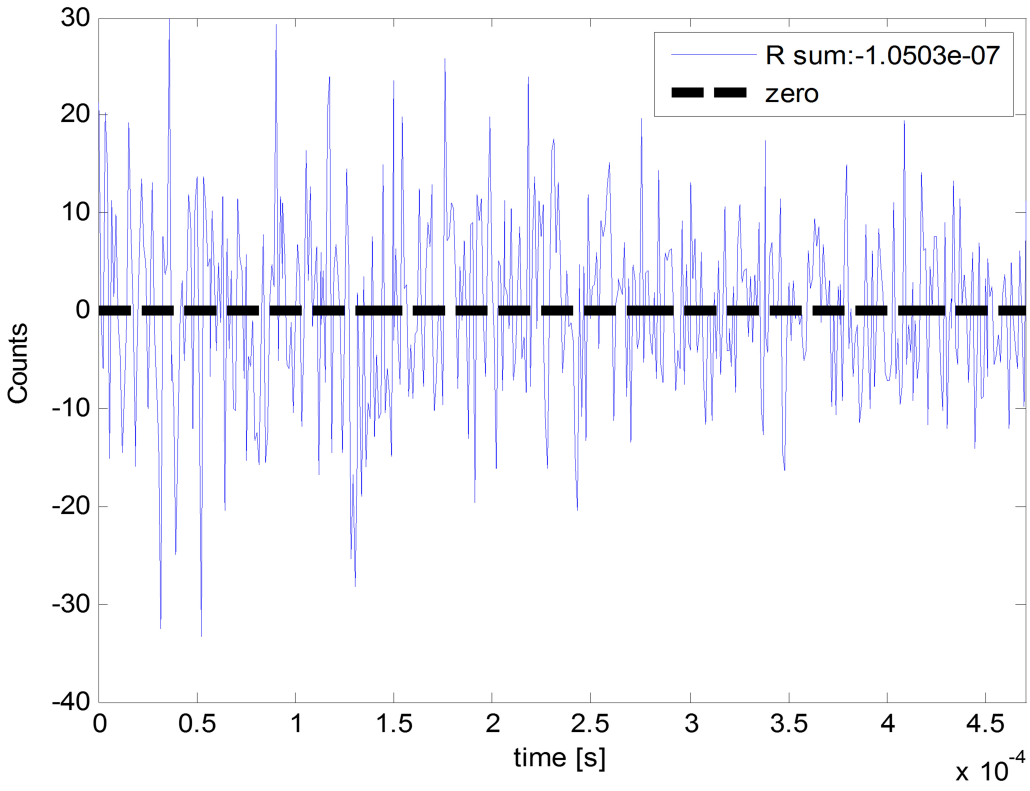


Figure 2.8: Optical lifetime measurement fitting residual shows the goodness of fitting with single exponential $I_o exp(-t/\tau)$.

wavelength 1280 nm. ZPL associated with (k) sites is labeled as $\beta$ lines and can be observed around wavelength 1335 nm [59].

The energy level of $V^{4+}$ is shown in figure 2.11. $V^{4+}$ has $3d^1$ electronic configuration and single electron doesn't experience repulsion, which is the simplest case considering energy levels. In Russel-Saunders coupling scheme, a free $V^{4+}$ ion takes only one energy level $^2D$. Under tetrahedral field, it splits to the ground state $^2E$ and the excited state $^2T_2$. In trigonal field, $^2T_2$ further splits to $^2E$ and $^2A_1$ states. With spin-orbit coupling, all states split into Kramers doublets. In the spectroscopy setup, we illuminated our sample with polarization perpendicular to c-axis and the middle transitions in four $\alpha$ lines are expected to be stronger due to orbitally allowed transitions.

The spin relaxation time $T_1$ around 4 K is 1 $\mu$s or shorter depending on lattice sites[60].

Table 1 Cr Lifetime on implanted 4H-SiC

| Temperature | Sample | Lifetime $\tau$ (us) | |
|---|---|---|---|
| | | $Cr_a$ | $Cr_c$ |
| RT | HPSI | 42.1 | 37.2 |
| | SI | 13.0 | 8.19 |
| LN T | HPSI | 49.8 | 53.0 |
| | SI | 26.6 | 26.0 |
| LHe T | HPSI | 48.9 | 52.5 |
| | SI | 30.5 | 40.1 |

Table 2 Cr Lifetime on doped 6H-SiC

| Temperature | Lifetime $\tau$ (us) | | |
|---|---|---|---|
| | $Cr_A$ | $Cr_B$ | $Cr_C$ |
| RT | 50.0 | 40.1 | 27.5 |
| LHe T | 147 | 153 | 137 |

Figure 2.9: Summary of optical lifetime measurements of $Cr^{4+}$ ions in implanted 4H-SiC and doped 6H-SiC samples at different temperature.

**$Mo^{5+}$ ions in 4H-SiC**

Photoluminescense associated with Mo ions were observed in 4H-SiC around 1076 nm as shown in 2.12. The corresponding configuration of Mo ions in 4H-SiC can be either substitutional or assymetric split vacancy [61] and different electric charge state, which have not been determined in previous works [62–64] until recent work using two laser spectroscopy under magnetic field [65]. The result indicates substitutional $Mo^{5+}$ at (h) site due to ground state Lande g-factor anisotropy. $Mo^{5+}$ has $4d^1$ electronic configuration, which results in the same energy level structure with $V^{4+}$ ions. The measured optical lifetime of excited state is 56 ns. The inhomogeneous spin coherence time $T_2^*$ is 320 ns [65].

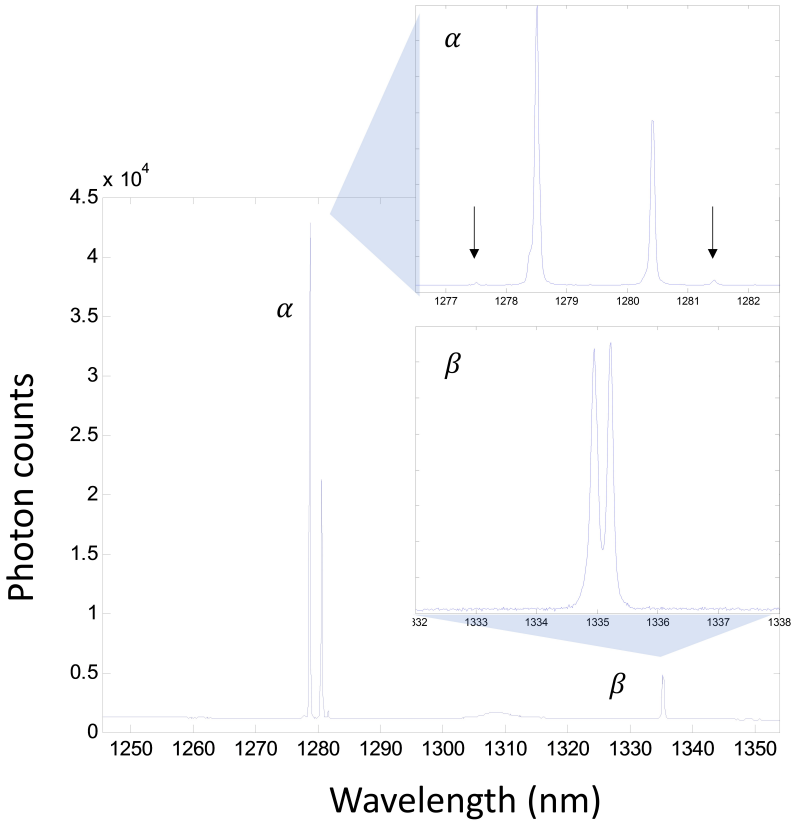


Figure 2.10: Photoluminescence of V ions in semi insulating 4H-SiC sample excited by 780 nm laser at liquid helium temperature.

**Cu in Si**

Cu in Si and exhibit bright and sharp photoluminescense around 1228 nm with optical lifetime 30 ns [66–68]. The PL spectra at different temperature are shown in figure 2.13 and 2.14. The spin relaxation or coherence time of these centers have not yet been investigated and the potential for qubits is still unknown.

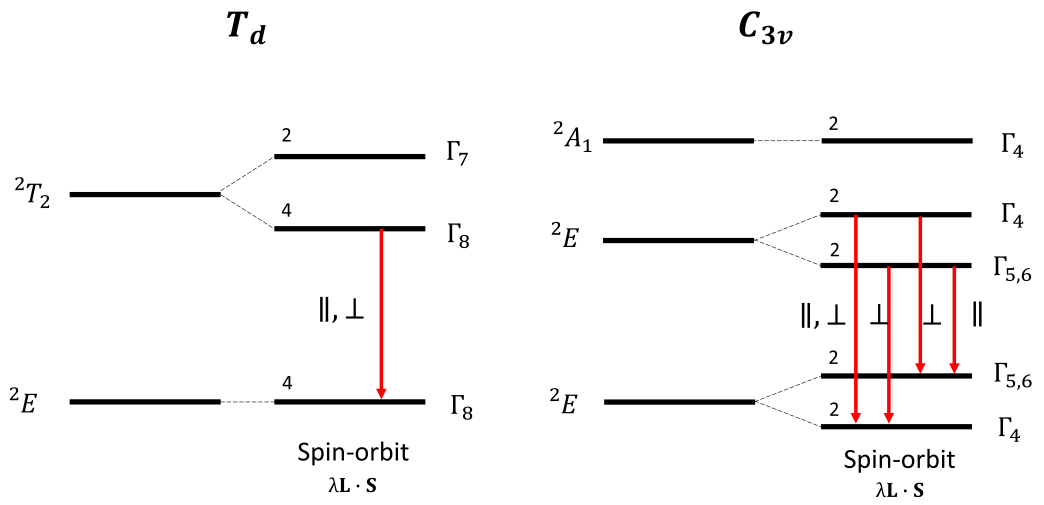


Figure 2.11: $V^{4+}$ energy level structure in 4H-SiC for $T_d$ and $C_{3v}$ symmetry. ZPL of $V^{4+}$ is associated with the transition $^2T_2 \longrightarrow {}^2E$. The number at left on level bars denotes state degeneracy and Γ specifies irreducible representation of corresponding symmetry group. Marks next to red arrows specify polarization of electric field to c-axis for electric dipole allowed transitions.

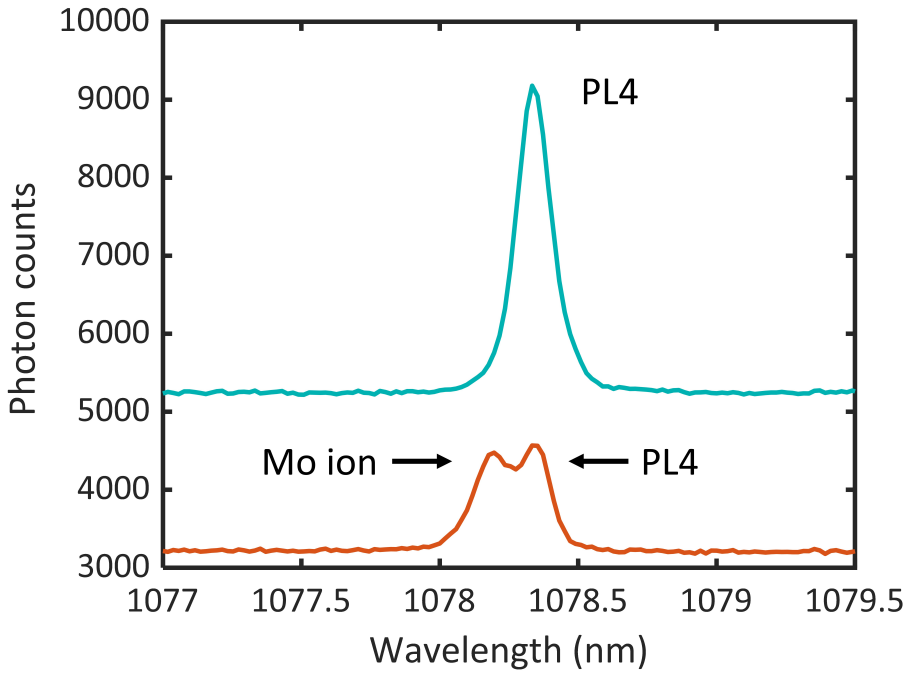


Figure 2.12: Photoluminescence of $Mo^{5+}$ ions in implanted sample (orange) in comparison with PL4 divacancies in a HPSi sample (blue) excited by 780 nm laser at 8.6K

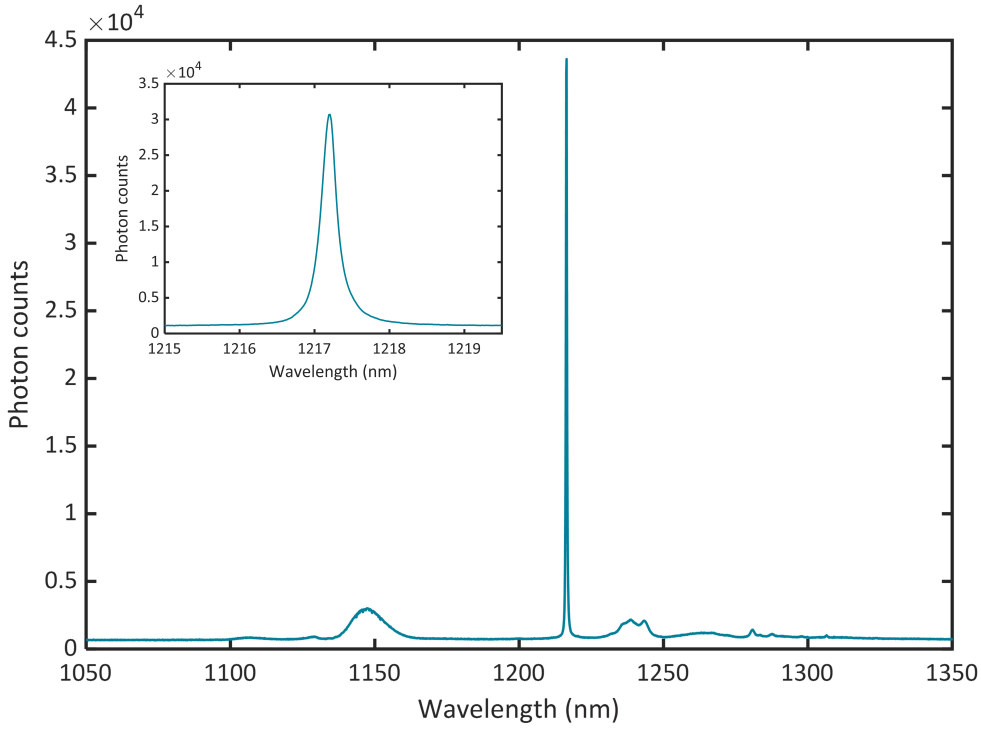


Figure 2.13: Photoluminescence of Cu ions in Cu implanted Si excited by 780 nm laser at 8.2K

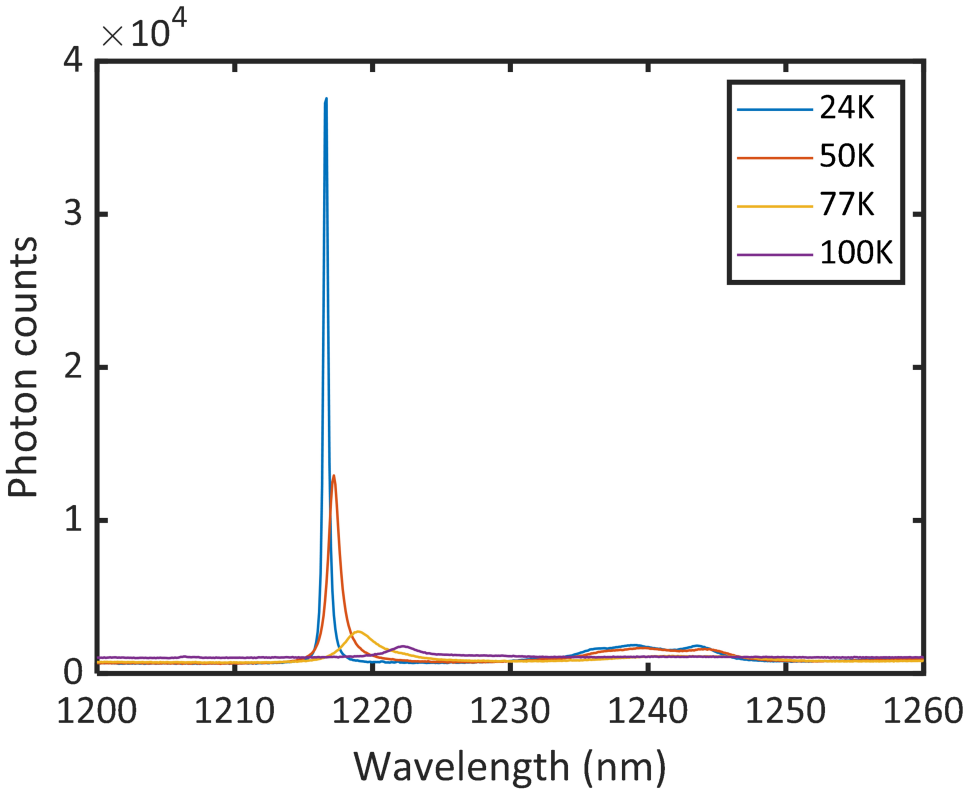


Figure 2.14: Photoluminescence of Cu ions in Cu implanted Si excited by 780 nm laser at different temperatures